Research Article | Vol. 26, No. 20 | 1 Oct 2018 | OPTICS EXPRESS 25667
Optics EXPRESS

Low loss Ge-on-Si waveguides operating in the 8–14 um atmospheric transmission window

K. GALLACHER,[1,3] R. W. MILLAR,[1,3] U. GRIŠKEVIČIŪTĖ,[1] L. BALDASSARRE,[2] M. SOREL,[1] M. ORTOLANI,[2] AND D. J. PAUL[1,*]

[1] *University of Glasgow, School of Engineering, Rankine Building, Oakfield Avenue, Glasgow, G12 8LT, UK*
[2] *Dipartimento di Fisica, Universita di Roma La Sapienza, Piazzale Aldo Moro 5, I-00185 Roma, Italy*
[3] *These authors contributed equally to the work*
[*] *Douglas.Paul@glasgow.ac.uk*

Abstract: Germanium-on-silicon waveguides were modeled, fabricated and characterized at wavelengths ranging from 7.5 to 11 μm. Measured waveguide losses are below 5 dB/cm for both TE and TM polarization and reach values of ~ 1 dB/cm for ≥ 10 μm wavelengths for the TE polarization. This work demonstrates experimentally for the first time that Ge-on-Si is a viable waveguide platform for sensing in the molecular fingerprint spectral region. Detailed modeling and analysis is presented to identify the various loss contributions, showing that with practical techniques losses below 1 dB/cm could be achieved across the full measurement range.

1. Introduction

Following the development of the silicon on insulator (SOI) integrated photonics platform at telecoms wavelengths, research has since shifted focus towards the mid-infrared part of the electromagnetic spectrum [1]. In this spectral region there is significant scope to create photonics circuits for molecular sensing [2], with potential applications in health-care, security (explosives [3,4] and chemical weapons [5,6] detection and identification) and environmental monitoring. The two major spectral regions of interest in the mid-infrared (MIR) for applications are the 3 to 5 μm, and 8 to 14 μm wavelength, low atmospheric absorption windows [7]. The 3 to 5 μm gas detection window has a wide range of gas detectors available with both sources and photodetectors for CO_2, O_2, CH_4 and many other small molecules [8]. The 8 to 14 μm window is much more important for larger molecules as many biological and chemical molecules have unique molecular absorption inside this window including the majority of explosives [3,4], chemical weapons [5,6], biological markers and pollutants. Indeed the 6.7 to 20 μm wavelength region is called the fingerprint region due to the ability to uniquely identify these molecules from absorption spectra.

For passive optics, low losses can only be achieved with the SOI platform up to ~ 3.6 μm, where absorption from the SiO_2 cladding begins to dominate [1]. Silicon-on-nothing platforms have been demonstrated with losses ≤ 3.1 dB/cm up to 7.67 μm wavelength [9]. The use of thick graded Si_yGe_{1-y} buffers have allowed SiGe waveguides to obtain losses as low ≤ 3 dB/cm from 5.5 to 8.5 μm wavelength but this required a ≥ 6 μm thick epitaxy layer which limits the integration options and will still be limited above 8.5 μm wavelength by Si absorption due to both impurity states and defect-activated multi-phonon absorption. Germanium has long been stated as an excellent material for a MIR photonics platforms [1]. It is Si compatible, transparent up to ~15 μm wavelength and has a significantly larger $\chi^{(3)}$ non-linearity than Si (at a given MIR wavelength) [10]. A number of Si compatible, MIR optical components have been demonstrated, including multi quantum well intersubband detectors [11], along with Ge plasmonics [3], and light emitters using GeSn [12, 13]. This makes Ge an ideal candidate for both passive structures and for supercontinuum generation in the MIR [14, 15], with the potential for creating MIR sensing systems on a Si platform. Ge waveguide losses have indeed been demonstrated in the

#334988 https://doi.org/10.1364/OE.26.025667
Journal © 2018 Received 13 Jun 2018; revised 15 Aug 2018; accepted 19 Aug 2018; published 18 Sep 2018

Optics EXPRESS

MIR [16] with multimode interfometers [17], ring resonators [18], and with demonstrations of sensing [19]. To date, however, there has only been experimental demonstration of MIR Ge waveguides up to 8.5 μm wavelength, where high losses ($\sim$ 20 dB/cm) were observed, with the most likely loss candidate being from free carrier absorption (FCA) due to background doping [20].

In this work, we demonstrate Ge-on-Si waveguides, characterized from 7.5 to 11 μm wavelength, with loss values below 5 dB/cm measured across the full range for TE and TM polarization. For wavelengths $\geq$ 10 μm the losses are found to reach as low as $\sim$ 1 dB/cm for the TE supported mode. These record losses are achieved by ensuring that Ge growth conditions minimize free carrier loss, which is critical in the MIR. Here, we undertake an analysis of the losses to determine the various contributing mechanisms, and highlight how the waveguide losses can be further reduced. To our knowledge these measurements demonstrate the lowest losses for an integrated dielectric waveguide on-chip $\geq$ 10 μm wavelength, and therefore confirms the feasibility of the Ge-on-Si platform for passive photonics operating in the 8 - 14 μm sensing window. The results and analysis indicate that sub-dB/cm losses are achievable across the full measurement range, with further optimization.

2. Growth and fabrication

2.1. Growth

Germanium epitaxial layers of 2 μm thickness were grown at IQE Silicon by reduced pressure - chemical vapor deposition (RP-CVD) on 150 mm diameter Si (001) Czochralski (Cz) substrates. The Si substrates have an electrical resistivity in the range of 10 - 20 Ω-cm, corresponding to a phosphorus doping concentration of $N_D \leq 5\times10^{14}$ cm^{-3}. The Ge layers were grown using the two temperature technique [21], and subsequently given thermal cyclic annealing to reduce the threading dislocation density (TDD) to $\leq 10^7$ cm^{-2} at the top plane. For the Ge growth, minimizing the background doping concentration is extremely important, as FCA follows a $\sim \lambda^2$ dependency, and is therefore non-negligible in the MIR even for moderate background densities [22]. It is also worth noting that for Ge, FCA is significantly higher in the MIR for p-type backgrounds compared to n-type of a similar concentration, mostly due to intra-valence band absorption [23, 24]. It is therefore critical that the growth chamber does not produce a high background p-type doping in the Ge if low waveguide losses are to be obtained. In addition, minimizing dopant segregation from the Si into the Ge epitaxial layer during growth is also an important consideration, and determines the choice of starting substrate. To illustrate the serious impact that moderate background doping densities can have on Ge waveguides in the 7 - 15 μm wavelength range, the FCA for n and p-type Ge of two different doping densities are plotted in Fig. 1, using data extracted from [22–25]. Figure 1 shows the absorption coefficient of doped Ge (dB/cm), however this could be considered as a waveguide loss for optical modes with a 100 % overlap with the Ge. It is evident that for a doping concentration of $\sim 3.2\times10^{15}$ cm^{-3}, a p-type background would result in propagation losses as large as $\sim$ 10 dB/cm in the range of 7.5 to 15 μm wavelength. For the equivalent n-type background the losses would be lower than $\sim$ 2.5 dB/cm across the same wavelength range. It should be noted that the n-type FCA can also be approximated using the model $\alpha_{fc}(cm^{-1}) = nK\lambda^a$, where n is the doping concentration (cm^{-3}) and λ is the wavelength (nm). For n-type Ge, $K \sim 5\times10^{-25}$, and $a \sim 2$ [22].

In this work, nominally un-doped Ge was targeted, however, for the reasons detailed above, we chose growth conditions that would be more likely to result in an n-type background, as opposed to p-type. This was achieved by selecting an n-type Si substrate and by using a growth reactor that had been predominately exposed to n-type dopants. To experimentally verify the dopant polarity of the 2 μm thick Ge epitaxial layer, the Seebeck effect (hot probe technique [26]) was used, and this confirmed the layer to be n-type. The background dopant concentration was then measured with secondary ion mass spectroscopy (SIMS) in a system with a phosphorous detection limit

Optics EXPRESS

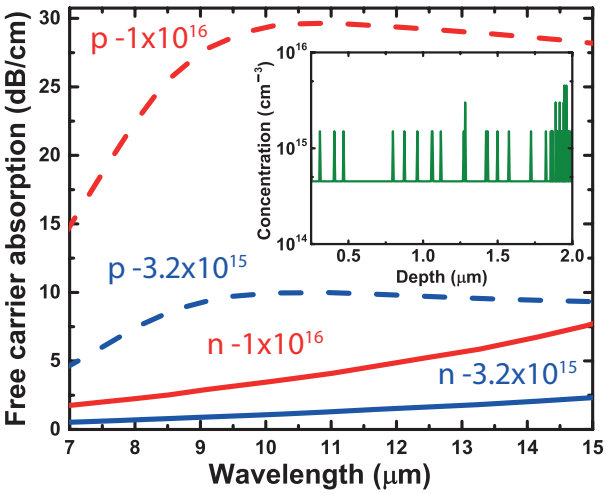

Fig. 1. The calculated free carrier absorption for different levels of n and p-type doping concentrations (units of cm^{-3}) in Ge. Data from [22–25]. The inset shows the secondary ion mass spectrometry measurement of the phosphorous doping concentration in the 2 μm thick Ge epitaxial layers.

(the n-type dopant predominately used in the growth chamber and in the Si substrate) down to 5×10^{14} cm^{-3} (EAG Laboratories). The inset of Fig. 1 demonstrates that the background doping concentration is equal to or below the noise of the SIMS measurements in the Ge epitaxial layer. At this level of n-type background doping, the waveguide losses caused by FCA should be negligible and the loss results presented later confirm this assumption.

2.2. Fabrication

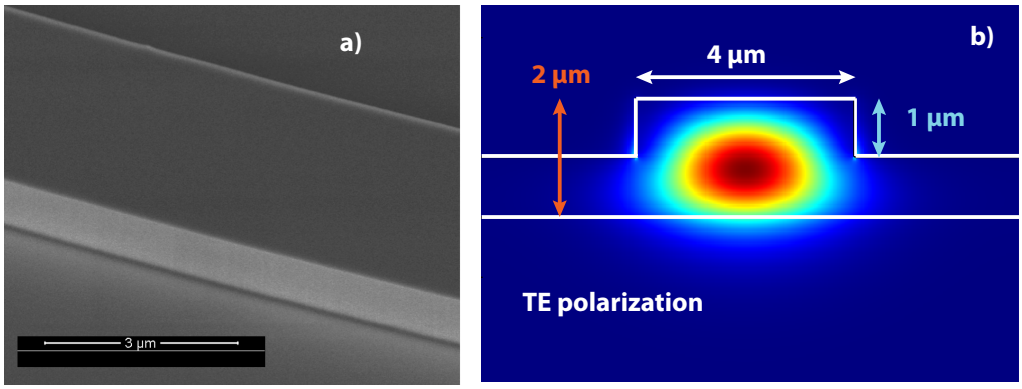

Fig. 2. (a) A scanning electron microscope image showing the sidewall of a 1 μm deep etched Ge-on-Si rib-waveguide. (b) The modeled TE mode profile for a Ge-on-Si rib-waveguide at 8 μm wavelength.

There are two main types of integrated waveguides that can be realized from a high index epilayer grown on a lower index substrate: ridge and rib waveguides. In ridge waveguides the guiding epilayer is fully etched down to the substrate level; in rib waveguides the epilayer is only partly etched (see Fig. 2). In this work, serpentine Ge rib waveguides with widths of 4 μm and lengths of 22.5 mm were patterned using ~ 650 nm thick hydrogen silsesquioxane (HSQ)

Optics EXPRESS

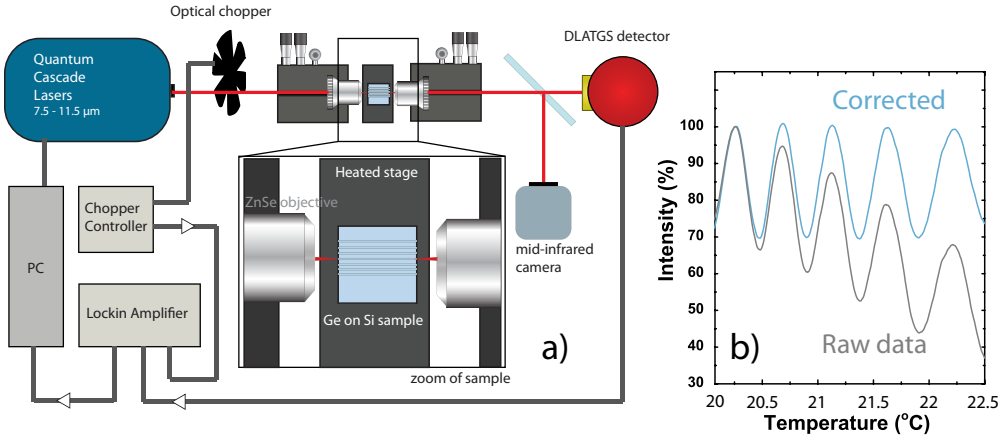

Fig. 3. (a) A schematic diagram showing the optical characterization setup. (b) The Fabry-Perot fringes observed from transmission through a 22.5 mm long Ge-on-Si rib waveguide, as the sample is thermally tuned. Thermal expansion of the stage causes a drift in the alignment, producing a slope in the raw data, which is subsequently corrected.

resist by electron-beam lithography. A technique was employed where the inner regions of the waveguides were written with a larger beam spot-size than the edges. This reduces electron beam lithography writing time while minimizing line-edge roughness. A waveguide width of 4 μm was chosen as this provides single mode operation across the full measurement range of the laser system (7.5 - 11.5 μm wavelength). The waveguides were patterned with linear tapers (reaching a width of 12.5 μm) in order to improve the input and output coupling efficiencies. The structures were subsequently dry etched to 1 μm depth in a mixed SF_6 and C_4F_8 recipe to form rib waveguides [27]. This recipe gives ~ 3.5:1 selectivity between HSQ and Ge. This etched height was measured by a surface profiler. As shown in Fig. 2(a), a scanning electron microscope image (SEM) demonstrates vertical sidewalls with minimal observable roughness. Rib waveguides have the advantage that they produce lower scattering losses from sidewalls, at the expense of tighter bend radii that can be achieved with ridge (fully etched) structures. Therefore, to minimize the bend loss in the serpentine structures, a large bending radius of 500 μm was chosen. A finite difference eigenmode modeling solver (Lumerical Mode Solutions) suggests that this radius should provide negligible bending loss.

3. Characterization

Waveguide loss measurements were undertaken using a Daylight Solutions MIRcat laser system containing four individual quantum cascade lasers (QCLs) providing a tunable continuous wave (cw) or pulsed source between 7.5 to 11.5 μm wavelengths. When operated in cw the QCLs provide a narrow line-width of $\leq$ 100 MHz. The QCL beam was focused onto a cleaved waveguide facet with a zinc selenide objective lens (NA = 0.25) and collected from the opposite facet using an identical objective. Alignment was achieved using an amorphous Si microbolometer camera (Xenics Gobi 640), and the signal was measured using a deuterated L-alanine doped triglycene sulphate (DLATGS) detector. The laser beam was modulated with an optical chopper, and the DLATGS detector was connected to a lock-in amplifier for both demodulation and data logging. The lock-in technique also ensured that the measurement discriminates against ambient black-body radiation.

Waveguide losses were calculated using the Fabry-Perot technique [28], which treats the waveguide as a cavity formed between the cleaved facets that act as mirrors. This technique is

Optics EXPRESS

especially suited to Ge since the frequency-independent high refractive index (~ 4) provides relatively high reflectance mirrors (~ 35 %) for measuring waveguide loss. Given that the QCLs in the setup are not continuously tunable without suffering from the effects of strong mode hopping, the wavelength was fixed at discrete measurement points. To observe the Fabry-Perot fringes the refractive index of the waveguide was instead tuned using the thermal-optic effect by using a resistive heater mounted onto the central 5 axis stage (Fig. 3(a)). The thermal-optic effect results in a refractive index change versus a change in temperature. Assuming the literature value for Ge in the MIR [29], the 22.5 mm long waveguides are expected to provide ~ two fringes per degree Celsius of heating. The sample temperature during heating was measured using the microbolometer camera, which has been calibrated for thermography and is accurate to ≤ 1 °C. The maximum temperature range for the measurement was limited by the thermal expansion of the stage, which caused optical misalignment of the waveguide with respect to the input and output objectives resulting in an observable slope in the measurement. This effect has also been reported in reference [16]. The slope induced in the intensity data is therefore corrected by fitting the successive minima of the fringes with a polynomial and subtracting the offset. The corrected fringes are subsequently normalized to the peak intensity before thermal misalignment. The thermal misalignment was also confirmed by using the QCL in pulsed operation, which increases the effective spectral bandwidth of the source and therefore suppresses the Fabry-Perot fringes. The resulting intensity plot versus heating was found to be consistent with the baseline fit to fringes using the fitting procedure.

An example of the Fabry-Perot fringes observed before and after correction is shown in Fig. 3(b). After measuring the Fabry-Perot fringes the waveguide loss is calculated using $\alpha(dB/cm) = -\frac{4.34}{L} ln\left(\frac{1}{R}\frac{\sqrt{\zeta}-1}{\sqrt{\zeta}+1}\right)$, where $\zeta = \frac{Intensity_{max}}{Intensity_{min}}$, R is the facet reflectivity and L is the waveguide length. The factor of 4.34 is required to convert the loss from cm^{-1} into dB/cm. The facet reflectivity has been calculated using the Fresnel equation with the effective index of the waveguide for TE and TM polarization at each measured wavelength. This calculation assumes perfect facets with zero roughness; this assumption will therefore overestimate the waveguide loss in the case of imperfect facets. It should also be noted that taper losses are also assumed to be zero; this ensures that our results do not underestimate the losses.

4. Results and analysis

Waveguide losses are demonstrated in Fig. 4(a) for the 4 μm wide Ge-on-Si rib waveguides. A solid line linking the data points is provided as an aid to the reader. Propagation losses are lower than 5 dB/cm for both TE and TM polarization across the full measurement range. For TM modes above 10 μm wavelength the signal to noise was too low to allow accurate measurement. This is most likely a consequence of the TM mode being close to cut-off, with > 50 % power in the Si substrate, coupled with lower laser powers from the relevant QCL chip. Significantly, however, from 10 to 11 μm wavelength the TE losses are as low as ~1 dB/cm, which to our knowledge is the lowest losses measured at such long wavelengths in the MIR for any integrated dielectric waveguide on-chip. It is also worth noting that the losses presented here for the TE modes from 7.5-11 μm wavelength are already in-line with losses typically associated with an established photonics platforms, such as SOI at telecommunication wavelengths [30]. This confirms that Ge-on-Si waveguides are indeed an excellent candidate for an integrated photonic waveguide platform for sensing.

For both TE and TM polarization, a clear peak in the waveguide loss spectra can be observed at 9.0 μm wavelength. This matches the shape of the Si-O-Si interstitial vibration; a molecular absorption state common in Cz grown Si where oxygen impurity levels can be ~ 10^{18} cm^{-3} [31]. This assertion is further evidenced by the reduction in loss observed at 9 μm wavelength for TE modes compared to TM, which have greater confinement in the Ge waveguide, and therefore

Optics EXPRESS

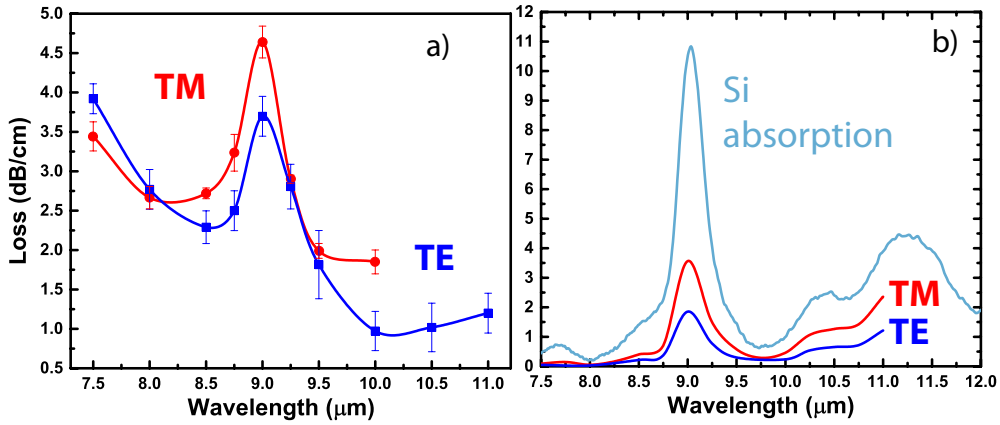

Fig. 4. (a) The propagation losses from a 4 μm wide Ge-on-Si rib waveguide for both transverse electric (TE) and transverse magnetic (TM) polarizations. The error bars denote the standard deviation of the losses calculated by successive Fabry-Perot fringes in the transmission measurement. (b) The Si substrate absorption measured by Fourier transform infrared spectroscopy. The corresponding waveguide loss caused by the optical overlap of the TE and TM modes in the Ge-on-Si rib waveguide with the Si substrate as modeled by Lumerical Mode Solutions.

a reduced optical overlap with the Si substrate. In order to decouple the various potential loss contributions, the optical constants of the Si substrate were measured by Fourier Transform Infrared (FTIR) spectroscopy using a Bruker IFS 66v FTIR with a liquid nitrogen cooled mercury cadmium telluride detector. The Ge epitaxial layer was selectively stripped in H_2O_2, which does not etch the underlying Si. Transmission and reflection spectroscopy measurements were undertaken in a quasi-normal incidence setup using a globar as the MIR optical source. This provides a measurement of the absorption coefficient when taking into account the slab reflection (R) and wafer thickness (d), by using $\alpha = -ln(T + R)/d$, where T is the measured transmission. The measured Si absorption coefficient is shown in Fig. 4(b), demonstrating absorption of ~ 10 dB/cm at ~ 9 μm wavelength. At longer wavelengths, multi-phonon absorption can be observed. Figure 4(b) also demonstrates the corresponding losses caused by the optical overlap with the Si substrate for both the supported single mode TE and TM polarizations for the 4 μm wide Ge-on-Si rib waveguides.

In order to establish the remaining source of waveguide loss, the calculated modal Si absorption was subtracted from the experimental data, Figs. 5(a) and 5(b). It is clear that this subtraction fully removes the local Si-O-Si molecular absorption peak in waveguide losses at 9 μm wavelength, validating the self consistency of the experiment and the modeling. From this subtraction, it is evident that the Si overlap is not the dominant contribution to waveguide losses, particularly at shorter wavelengths than the interstitial oxygen vibration at ~ 9 μm wavelength. The slope of the residual losses is in fact indicative of sidewall scattering, with similarity to the Payne and Lacey model [32], which is shown in the right of Fig. 5(c). The Payne and Lacey model was first developed to describe scattering losses in 2-d slab waveguides with roughness at the top and bottom interfaces, and has since been modified for 3-d structures. In this model, only the line-edge roughness (anisotropic) is described. It is also only relevant for fully etched (ridge) waveguides and has therefore only been included to demonstrate an approximate trend of loss with wavelength, and the approximate level of scattering losses for a given roughness in the MIR. Future work is required with finite difference time domain (FDTD) modeling to determine how this loss scales in rib structures, which is beyond the scope of this work. The modified Payne

Optics EXPRESS

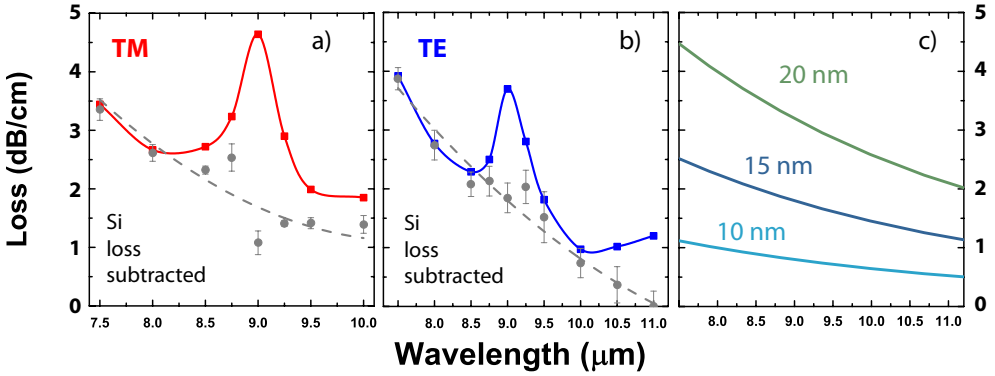

Fig. 5. (a) and (b) The measured waveguide loss (solid lines) and the calculated loss following the subtraction of the Si absorption (grey dashed lines), for TM and TE modes respectively. The data points are fitted with a second order polynomial. (c) The scattering losses as calculated by an analytical scattering model (Payne and Lacey) for a 4 μm wide fully etched ridge Ge-on-Si waveguide for three different rms roughness amplitude values. A correlation length of 150 nm was used.

and Lacey model was implemented and then validated using a range of other experimental data at various wavelengths [28, 30, 33], and it was confirmed to provide a good correlation to these experimental results. The loss from sidewall scattering in the present work is further evidenced by the increased loss at shorter wavelengths for TE modes (compared to TM), which are known to be more severely affected by surface roughness. While waveguide loss via sidewall scattering is usually assumed to be negligible at longer wavelengths, the high refractive index difference between the Ge and air of $\Delta n \sim 3$ compared to Si, SiGe and many III-V materials can still cause significant propagation losses with even moderate levels of root mean square (rms) roughness amplitude (> 10 nm). For example, as shown in Fig. 5(c), for a 2 μm thick, 4 μm wide ridge waveguide with 20 nm rms roughness amplitude can cause ~ 4.5 dB/cm scattering losses at 7.5 μm wavelength. This assumes a correlation length of 150 nm (which is typical for electron beam lithography systems).

5. Discussion

There are a number of approaches by which the observed scattering losses can be reduced. The waveguide width can be optimized for the given wavelength of operation, which reduces the modal overlap with the sidewalls thereby reducing sidewall scattering loss. Furthermore, electron beam lithography techniques such as "multi-pass" can be used to reduce sidewall roughness by averaging beam-current errors. Oxidation of waveguide sidewalls has previously been shown to reduce scattering in Si waveguides [28], however with thermal Ge oxide [34], it would have to subsequently be stripped as it is not transparent in the MIR. Finally, the use of a suitable MIR-transparent cladding layer can reduce the Δn, and consequently the scattering loss. Reducing the sidewall roughness to 10 nm would bring the scattering loss at 7.5 μm to ~ 1 dB/cm, and to ~ 0.5 dB/cm at 11 μm wavelength. For rib structures these losses would be further reduced. In terms of reducing the loss from Si absorption, there are multiple approaches that can be taken. Thicker Ge epitaxial layers will provide greater modal confinement, therefore reducing the Si modal overlap. The dominant loss mechanism in the Si substrate between 8 and 15 μm wavelength is in fact the vibration due to interstitial oxygen; this can be almost fully eliminated by using Float Zone (Fz) Si substrates. There is also the potential that misfits and threading dislocations that form during growth may contribute to the losses. However, to quantify this

effect would require multiple growths with varying dislocation density. This will be the subject of future work. Finally, there is potential for Ge-on-nothing structures where the Si is selectively removed underneath the waveguide. These preliminary results are therefore extremely promising in demonstrating that Ge-on-Si can be an effective MIR sensing platform in the 8 to 14 μm atmospheric transmission window.

6. Conclusion

The first demonstration of low loss Ge-on-Si mid-infrared waveguides operating in the wavelength range of 7.5 - 11 μm is presented. Losses below 5 dB/cm are found for both TE and TM polarizations in the rib waveguide structures, with 2 μm thickness, etched to a depth of 1 μm. In particular, losses below 3 dB/cm are found between 9.25 and 11 μm wavelength and around 1 dB/cm for TE polarization modes of 10 μm and above. For both polarizations, the effect of Si absorption can be observed, particularly at 9 μm wavelength where there is strong absorption from an interstitial oxygen vibration. In order to decouple the various potential loss mechanisms, the Si absorption was experimentally measured, and the effect of Si absorption was subtracted from the propagation loss. The residual losses observed are not due to free carrier absorption, as confirmed by SIMS measurements. In conclusion, the experiment trend appears consistent with sidewall scattering losses, and therefore this suggests that practical techniques such as application of cladding layers and improvement of lithographic processes can be used to reduce the losses further to below 1 dB/cm across the full range of 7.5 to 11 μm. This work provides the first experimental evidence that low loss Ge waveguides are practically achievable in the 8-14 μm atmospheric transmission window.

Funding

This work was funded by EPSRC grant EP/N003225/1. M. O. and L. B. acknowledge support from the Italian Ministry of University and Research, program SIR, Grant no. RBSI14IT0D.

Acknowledgments

The authors would like to thank the staff of the James Watt Nanofabrication Centre for their assistance with the fabrication.

References

1. R. Soref, "Mid-infrared photonics in silicon and germanium," Nat. Photonics **4**, 495–497 (2010).
2. B. Schwarz, P. Reininger, D. Ristanić, H. Detz, A. M. Andrews, W. Schrenk, and G. Strasser, "Monolithically integrated mid-infrared lab-on-a-chip using plasmonics and quantum cascade structures," Nat. Commun. **5**, 4085 (2014).
3. L. Baldassarre, E. Sakat, J. Frigerio, A. Samarelli, K. Gallacher, E. Calandrini, G. Isella, D. J. Paul, M. Ortolani, and P. Biagioni, "Midinfrared plasmon-enhanced spectroscopy with germanium antennas on silicon substrates," Nano Lett. **15**, 7225–7231 (2015).
4. P. M. Pellegrino, E. L. Holthoff, and M. E. Farrell, eds., *Laser Based Optical Detection of Explosives* (CRC, 2017).
5. E. R. Deutsch, P. Kotidis, N. Zhu, A. K. Goyal, J. Ye, A. Mazurenko, M. Norman, K. Zafiriou, M. Baier, and R. Connors, "Active and passive infrared spectroscopy for the detection of environmental threats," Proc. SPIE **9106**, 9106 – 9106 – 10 (2014).
6. D. J. Paul, K. Gallacher, R. W. Millar, V. Giliberti, E. Calandrini, L. Baldassarre, M. P. Fischer, J. Frigerio, A. Ballabio, E. Sakat, G. Pellegrini, D. Brida, G. Isella, M. Ortolani, and P. Biagioni, "n-Ge on Si for mid-infrared plasmonic sensors," in *2017 IEEE Photonics Society Summer Topical Meeting Series (SUM),* (2017), pp. 125–126.
7. L. Rothman, I. Gordon, Y. Babikov, A. Barbe, D. C. Benner, P. Bernath, M. Birk, L. Bizzocchi, V. Boudon, L. Brown, A. Campargue, K. Chance, E. Cohen, L. Coudert, V. Devi, B. Drouin, A. Fayt, J.-M. Flaud, R. Gamache, J. Harrison, J.-M. Hartmann, C. Hill, J. Hodges, D. Jacquemart, A. Jolly, J. Lamouroux, R. L. Roy, G. Li, D. Long, O. Lyulin, C. Mackie, S. Massie, S. Mikhailenko, H. Müller, O. Naumenko, A. Nikitin, J. Orphal, V. Perevalov, A. Perrin, E. Polovtseva, C. Richard, M. Smith, E. Starikova, K. Sung, S. Tashkun, J. Tennyson, G. Toon, V. Tyuterev, and G. Wagner, "The HITRAN2012 molecular spectroscopic database," J. Quant. Spectrosc. Radiat. Transf. **130**, 4 – 50 (2013).

Optics EXPRESS

8. J. Chou, *Hazardous Gas Monitors: A Practical Guide to Selection, Operation, and Applications* (McGraw-Hill, New York, USA, 2000).
9. J. S. Penadés, A. Sánchez-Postigo, M. Nedeljkovic, A. Ortega-Monux, J. G. Wangüemert-Pérez, Y. Xu, R. Halir, Z. Qu, A. Z. Khokhar, A. Osman, W. Cao, C. G. Littlejohns, P. Cheben, I. Molina-Fernández, and G. Z. Mashanovich, "Suspended silicon waveguides for long-wave infrared wavelengths," Opt. Lett. **43**, 795–798 (2018).
10. N. K. Hon, R. Soref, and B. Jalali, "The third-order nonlinear optical coefficients of Si, Ge, and $Si_{1-x}Ge_x$ in the midwave and longwave infrared," J. Appl. Phys. **110**, 011301 (2011).
11. K. Gallacher, A. Ballabio, R. W. Millar, J. Frigerio, A. Bashir, I. MacLaren, G. Isella, M. Ortolani, and D. J. Paul, "Mid-infrared intersubband absorption from p-Ge quantum wells grown on Si substrates," Appl. Phys. Lett. **108**, 091114 (2016).
12. R. W. Millar, D. C. S. Dumas, K. F. Gallacher, P. Jahandar, C. MacGregor, M. Myronov, and D. J. Paul, "Mid-infrared light emission > 3 μm wavelength from tensile strained GeSn microdisks," Opt. Express **25**, 25374–25385 (2017).
13. J. Margetis, S. Al-Kabi, W. Du, W. Dou, Y. Zhou, T. Pham, P. Grant, S. Ghetmiri, A. Mosleh, B. Li, J. Liu, G. Sun, R. Soref, J. Tolle, M. Mortazavi, and S.-Q. Yu, "Si-Based GeSn lasers with wavelength coverage of 2 - 3 μm and operating temperatures up to 180 K," ACS Photonics **5**, 827–833 (2018).
14. M. Sinobad, C. Monat, B. Luther-davies, P. Ma, S. Madden, D. J. Moss, A. Mitchell, D. Allioux, R. Orobtchouk, S. Boutami, J.-M. Hartmann, J.-M. Fedeli, and C. Grillet, "Mid-infrared octave spanning supercontinuum generation to 8.5 μm in silicon-germanium waveguides," Optica **5**, 360–366 (2018).
15. M. Yang, Y. Guo, J. Wang, Z. Han, K. Wada, L. C. Kimerling, A. M. Agarwal, J. Michel, G. Li, and L. Zhang, "Mid-IR supercontinuum generated in low-dispersion Ge-on-Si waveguides pumped by sub-ps pulses," Opt. Express **25**, 16116 (2017).
16. Y.-C. Chang, V. Paeder, L. Hvozdara, J.-M. Hartmann, and H. P. Herzig, "Low-loss germanium strip waveguides on silicon for the mid-infrared." Opt. Lett. **37**, 2883–2885 (2012).
17. M. Nedeljkovic, J. S. Penadés, C. J. Mitchell, A. Z. Khokhar, S. Stankovic, T. D. Bucio, C. G. Littlejohns, F. Y. Gardes, and G. Z. Mashanovich, "Surface-grating-coupled low-loss Ge-on-Si rib waveguides and multimode interferometers," IEEE Photonic Tech L **27**, 1040–1043 (2015).
18. B. Troia, J. S. Penades, A. Z. Khokhar, M. Nedeljkovic, C. Alonso-Ramos, V. M. N. Passaro, and G. Z. Mashanovich, "Germanium-on-silicon vernier-effect photonic microcavities for the mid-infrared," Opt. Lett. **41**, 610–613 (2016).
19. Y. C. Chang, P. Wägli, V. Paeder, A. Homsy, L. Hvozdara, P. Van Der Wal, J. Di Francesco, N. F. De Rooij, and H. Peter Herzig, "Cocaine detection by a mid-infrared waveguide integrated with a microfluidic chip," Lab Chip **12**, 3020–3023 (2012).
20. M. Nedeljkovic, J. S. Penades, V. Mittal, G. S. Murugan, A. Z. Khokhar, C. Littlejohns, L. G. Carpenter, C. B. E. Gawith, J. S. Wilkinson, and G. Z. Mashanovich, "Germanium-on-silicon waveguides operating at mid-infrared wavelengths up to 8.5 μm," Opt. Express **25**, 27431–27441 (2017).
21. L. Colace, G. Masini, F. Galluzzi, G. Assanto, G. Capellini, L. D. Gaspare, E. Palange, and F. Evangelisti, "Metal-Ge-Si heterostructures for near-infrared light detection," J. Vac. Sci. Technol. B **17**, 465–467 (1999).
22. J. I. Pankove, *Optical Processes in Semiconductors* (Dover, 1971).
23. R. Newman and W. W. Tyler, "Effect of impurities on free-hole infrared absorption in p-type germanium," Phys. Rev. **105**, 885–886 (1957).
24. M. Nedeljkovic, R. Soref, and G. Z. Mashanovich, "Predictions of free-carrier electroabsorption and electrorefraction in germanium," IEEE Photonics J. **7**, 1–14 (2015).
25. H. B. Briggs and R. C. Fletcher, "New infrared absorption bands in p-type germanium," Phys. Rev. **87**, 1130–1131 (1952).
26. D. K. Schroder, *Semiconductor Material and Device Characterization* (Wiley Interscience, 2006), 3rd ed.
27. M. M. Mirza, H. Zhou, P. Velha, X. Li, K. E. Docherty, A. Samarelli, G. Ternent, and D. J. Paul, "Nanofabrication of high aspect ratio (~50:1) sub-10 nm silicon nanowires using inductively coupled plasma etching," J. Vac. Sci. Technol. B **30**, 06FF02 (2012).
28. D. K. Sparacin, S. J. Spector, and L. C. Kimerling, "Silicon waveguide sidewall smoothing by wet chemical oxidation," J. Light. Technol. **23**, 2455–2461 (2005).
29. H. H. Li, "Refractive index of silicon and germanium and its wavelength and temperature derivatives," J. Phys. Chem. Ref. Data **9**, 561–658 (1980).
30. C. Bellegarde, E. Pargon, C. Sciancalepore, C. Petit-Etienne, V. Hugues, D. Robin-Brosse, J. M. Hartmann, and P. Lyan, "Improvement of sidewall roughness of submicron SOI waveguides by hydrogen plasma and annealing," IEEE Photon. Technol. Lett. **30**, 591–594 (2018).
31. R. C. Newman, "Oxygen diffusion and precipitation in Czochralski silicon," J. Physics: Condens. Matter **12**, R335 (2000).
32. F. P. Payne and J. P. R. Lacey, "A theoretical analysis of scattering loss from planar optical waveguides," Opt. Quantum Electron. **26**, 977–986 (1994).
33. D. E. Hagan and A. P. Knights, "Mechanisms for optical loss in SOI waveguides for mid-infrared wavelengths around 2 μm," J .Opt. **19**, 025801 (2017).
34. F. Pezzoli, A. Giorgioni, K. Gallacher, F. Isa, P. Biagioni, R. W. Millar, E. Gatti, E. Grilli, E. Bonera, G. Isella, D. J. Paul, and L. Miglio, "Disentangling nonradiative recombination processes in Ge micro-crystals on Si substrates," Appl. Phys. Lett. **108**, 262103 (2016).